High-Efficiency All-Polymer Solar Cells Based on a Pair of Crystalline Low-Bandgap Polymers

Cheng Mu, Peng Liu, Wei Ma, Kui Jiang, Jingbo Zhao, Kai Zhang, Zhihua Chen, Zhanhua Wei, Ya Yi, Jiannong Wang, Shihe Yang, Fei Huang,* Antonio Facchetti, Harald Ade,* and He Yan**

During the past decade, polymer solar cells (PSCs)[1–4] have attracted considerable academic and industrial attention due to their potential for low-cost solar energy production. Best-performing PSCs consist of a p-type semiconducting polymer as the electron donor and a fullerene derivative as the electron acceptor. Despite the essential role of fullerenes in a PSC, they have several drawbacks such as poor light absorption and high production costs (e.g., $PC_{71}BM$). On the other hand, PSCs based on a polymer donor and a polymer acceptor (referred to as all-polymer solar cells, all-PSCs) are emerging as a promising class of devices as polymers offer broadened absorptions and more flexibility in tuning the chemical structures and thus the energy levels of the donor and acceptor components.[5–10] Driven by these promises, there have been intensive research efforts in all-PSCs, with efficiencies of 3.0–4.4% achieved by a few research groups.[6–9,11] The best efficiency of all-PSCs, however, remains significantly lower than that of state-of-the-art polymer:fullerene PSCs. Besides polymer acceptors, small molecule acceptors have also been explored as alternatives to fullerenes.[12–17]

A common approach to improve the efficiency of polymer:fullerene PSCs is by using donor polymers with relatively low optical bandgaps.[4,18–25] In the area of all-PSCs, much progress has been made by understanding and controlling the degree of aggregation and the morphology of donor:acceptor blends,[26–29] but there are few examples of low-bandgap (<1.6 eV) donor polymers utilized for high-efficiency all-PSCs. 30-34 Due to the suboptimal bandgaps of donor polymers and/or relatively low external quantum efficiencies (EQEs) of the cells, the J_{sc} of all-PSCs have been limited so far to ~7–9 mA cm^{-2}. This is a key difference between all-PSCs and polymer:fullerene PSCs, as the latter can achieve high EQE and large absorption width at the same time, leading to J_{sc} larger than 15 mA cm^{-2} for the best cells.[3] Besides low-bandgap, several other important requirements to achieving high-efficiency all-PSCs include a favorable polymer:polymer morphology and high charge transport mobilities for the polymers. In general, all-PSC are based on highly complicated material systems that depend upon many parameters (such as bandgap, morphology, charge transport, etc).

Here we report high-performance all-PSCs with an average efficiency of 4.7% (best efficiency, 5.0%, **Table 1**) utilizing the combination of a naphthobisthiadiazole-benzodithiophene low-bandgap (1.58 eV) donor polymer indicated here as NT[19,35] and the naphthalenediimide-bithiophene n-type semiconducting polymer P(NDI2OD-T2), also known as Activink N2200[36] (**Figure 1**a). **Figure 2**a shows the optical absorption spectra of neat NT and N2200 films as well as that of the blend film (1:1 weight ratio of NT and N2200) all having a similar thickness of ~90 nm. The main optical absorption peaks of NT and N2200 are largely overlapping. Inverted solar cell devices were fabricated using ZnO as the cathode interlayer and V_2O_5/Al as the anode. The current density/voltage (*J-V*) curves of one of the best NT:N2200 cells is shown in Figure 2b, which exhibits a J_{SC} = 11.5 mA cm^{-2}, a V_{OC} = 0.77 V, a FF = 0.56, and a PCE = 5.0%

Table 1. Performance of NT:N2200-based PSCs with different D:A ratios and related PSCs for comparison. Presented were average data over 10 devices. The solvent used is 1,2-dichlorobenzene (DCB), except for the last row; and devices were anneal at 160–180 °C, except for the first row.

Blend weight ratio	V_{OC} [V]	J_{SC} [mA cm^{-2}]	FF	PCE [%]
NT:N2200 = 1:1	0.76 ± 0.01	8.2 ± 0.2	0.41 ± 0.05	2.6 ± 0.3[a)]
NT:N2200 = 1:1	0.77 ± 0.01	11.3 ± 0.2	0.53 ± 0.04	4.7 ± 0.3
NT:N2200 = 3:2	0.76 ± 0.01	10.4 ± 0.5	0.44 ± 0.02	3.5 ± 0.2
NT:N2200 = 2:3	0.77 ± 0.01	9.7 ± 0.2	0.51 ± 0.04	3.8 ± 0.2
NT:N2200 = 1:1	0.74 ± 0.01	8.2 ± 0.4	0.44 ± 0.04	2.7 ± 0.2[b)]

[a)]These devices were not thermally annealed; [b)]These devices were processed from the tetralin solution of NT:N2200.

C. Mu, K. Jiang, J. Zhao, Z. Wei, S. Yang, H. Yan
Department of Chemistry
Hong Kong University of Science and Technology
Clear Water Bay, KowLoon, Hong Kong, China
E-mail: hyan@ust.hk
P. Liu, K. Zhang, F. Huang
Institute of Optoelectronic Materials and Devices
State Key Laboratory of Luminescent Materials and Devices
South China University of Technology Guangzhou
510640, P. R. China
E-mail: msfhuang@scut.edu.cn
W. Ma,[†] H. Ade
Department of Physics
North Carolina State University
Raleigh, NC 27695, USA
E-mail: wma5@ncsu.edu; hwade@ncsu.edu
Z. Chen, A. Facchetti
Polyera Corporation
8045 Lamon Avenue, Skokie, Illinois 60077, USA
Y. Yi, J. Wang
Department of Physics
Hong Kong University of Science and Technology
Clear Water Bay, KowLoon, Hong Kong, China
[†]Current address: XJTU-HKUST Joint School of Sustainable Development, Xi'an Jiaotong University, Xi'an, P.R. China

DOI: 10.1002/adma.201402473

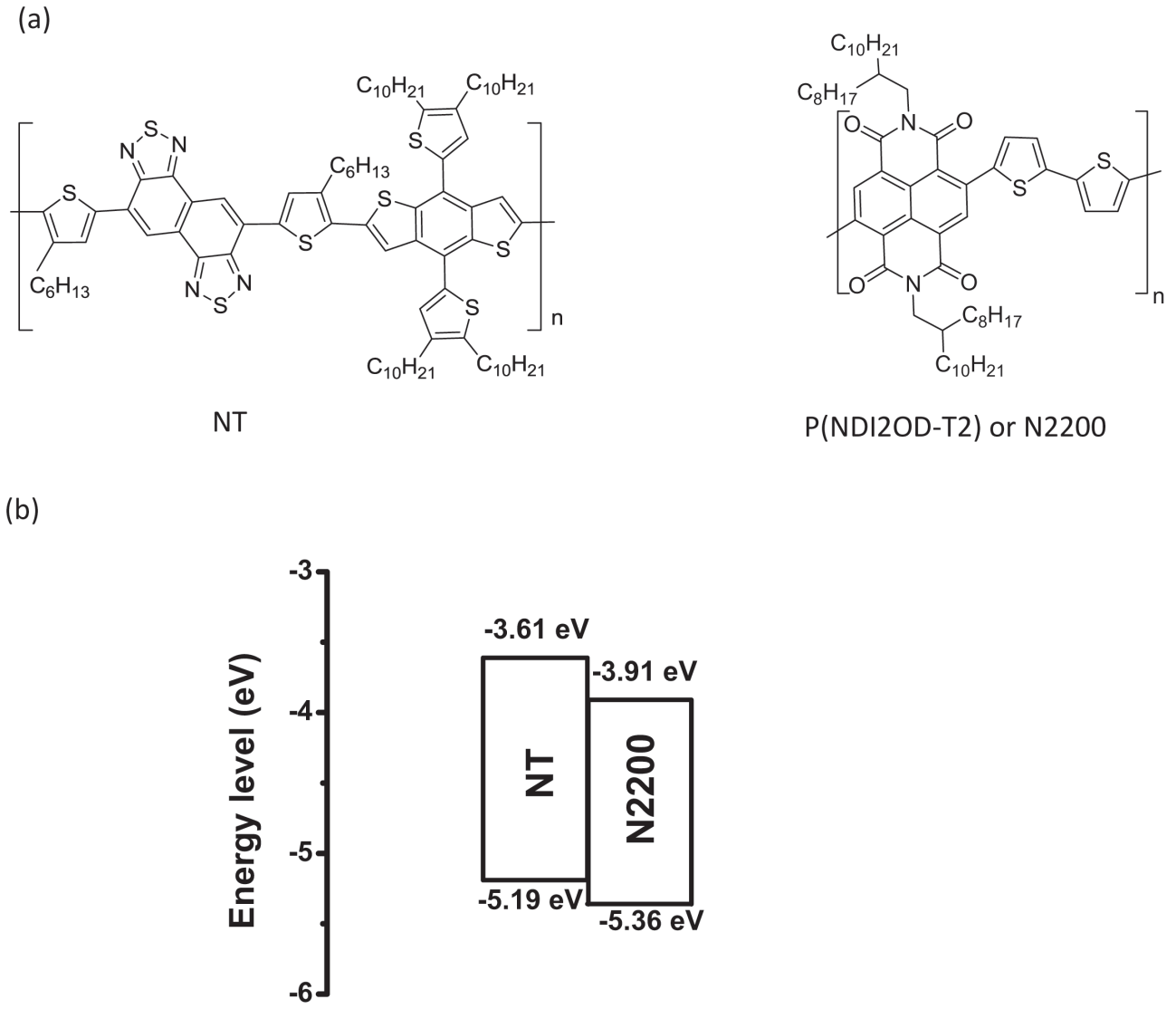

Figure 1. (a) Chemical structures of NT and N2200; (b) energy levels of NT and N2200; the HOMO and LUMO levels of N2200 and HOMO level of NT were taken from the literature. The LUMO level of NT was estimated from its HOMO and optical bandgap.

(Table 1). The average EQE (Figure 2c) of NT:N2200-based cells can reach about 40–50%, which, combined with the large absorption width of NT, leads to a J_{sc} of about 11.5 mA cm^{-2}. The V_{OC} of NT:N2200-based all-PSCs is respectably high (0.78 V) due to the low-lying HOMO level of NT relative to the LUMO level of N2200 (Figure 1b). Extensive device and process optimizations have been carried out by changing the D:A ratio, annealing temperature, processing solvents, additives, and device structures. NT:N2200-based PSCs with various donor:acceptor ratios are shown in Table 1, with the 1:1 ratio achieving the highest PCE. Thermal annealing of the NT:N2200 blend film at 160–180 °C can increase the PCE (Table 1) significantly due to increased molecular ordering/crystalliziation, which in turn improves charge transport ability of the polymer blend (which will be discussed later) and thus results in enhanced FF. Performances of all-PSCs with different solvents, additive, and device structures are summarized (Table S1) and explained in the Supporting Information.

Resonant soft X-ray scattering (R-SoXS) has been demonstrated to be one of the few tools capable to probe the phase separation in polymer:polymer blend films.[37–39] The scattering contrast between NT and N2200 is plotted in Figure S1, normalized to the mass-thickness contrast of N2200. The relative contrast is highest at 284–286 eV and these energies are thus most suited to investigate the domain structure. An energy just below the contrast peak is used in order to avoid strong absorption, which results in a fluorescent background and radiation damage. The brown line in **Figure 3**a shows the R-SoXS profiles at 284.2 eV for an NT:N2200 blend film processed from DCB. A scattering peak is observed at q≈0.02–0.03 nm^{-1}, corresponding to the NT:N2200 phase separation. The median domain separation can be estimated to be ~200 nm, which is

Adv. Mater. **2014**,
DOI: 10.1002/adma.201402473

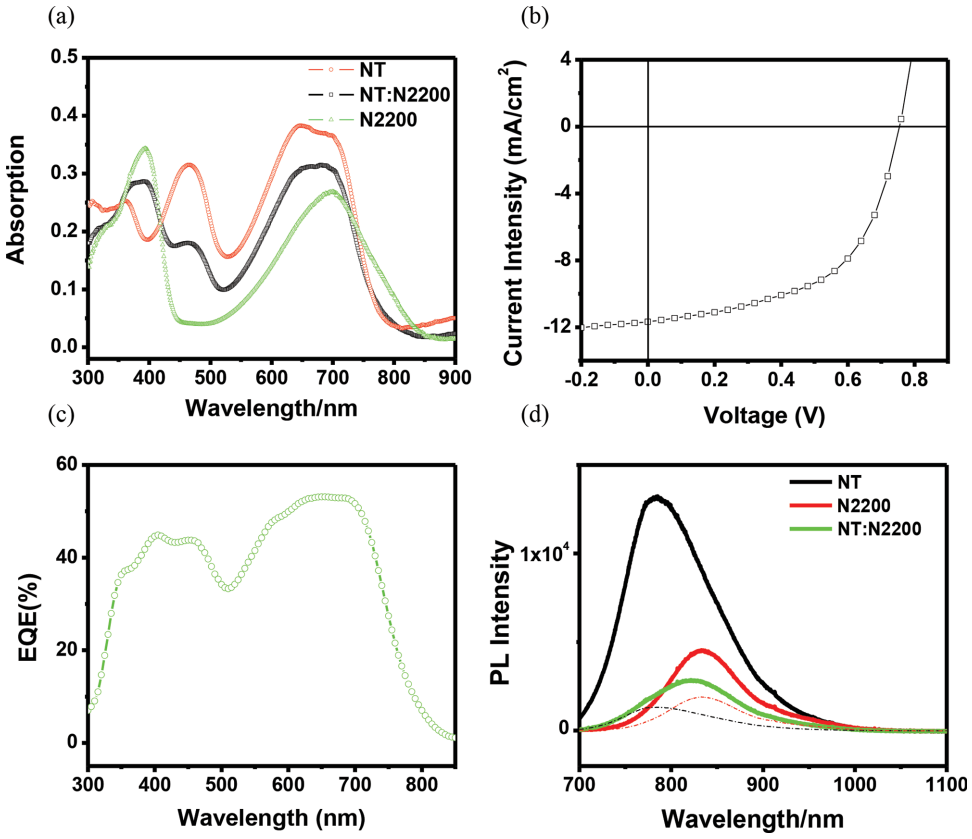

Figure 2. (a) Absorption spectra of NT, N2200 and N2200:NT films with 90 nm thickness; (b) J–V curves for an NT:N2200-based all-PSC (1:1, w/w); (c) EQE spectrum of NT:N2200-based all-PSC. (d) Photoluminescence (PL) spectrum of a NT:N2200 blend film (green line) compared with PL spectra of NT (black line) and N2200 (red line) control films. The dashed black line shows the NT component peak of the NT:N2200 PL emission peak, and the dashed red line shows the N2200 component peak of the NT:N2200 PL emission peak.

approximately twice the median domain size since there are roughly equal volume fractions of the two respective polymer-rich domains in the blend. Therefore, the median domain size of NT:N2200 blend processed from DCB should be ~100 nm. In addition, neither atomic force microscopy (AFM) nor transmission electron microscopy (TEM) images of the NT:N2200 blend film show obvious features larger than 100 nm (Figure S2). The AFM images show fibrillar textures with feature sizes of about 30–40 nm, which is typically observed for N2200-based pure or blend films and possibly reflects crystallites within larger polymer domains. The features shown in TEM images are smaller than 50 nm. Note that AFM is only surface sensitive and TEM provides the projection images of the film and is mostly sensitive to density contrast, i.e. mass-thickness contrast. In contrast, R-SoXS provides information about average domain size of the compositional variations in the bulk of the film without convoluting any vertical overlap of domains. Although the domain size (100 nm) of NT:N2200 is relatively large, it is quite comparable to the domain size (80 nm) of NT:PC_{71}BM blends, which can yield reasonably high PSC efficiency due to the impure nature of NT polymer domains.[37] Photoluminescence quenching experiments showed that the photoluminescence quenching efficiency (PLQE) of NT in the NT:N2200 blend (1:1 weight ratio) is ~90%, while the PLQE of N2200 in the same NT:N2200 film is 58% (Figure 2d). These PLQE results are similar to previous observations on PTQ1:N2200[9] and P3HT:N2200 blends.[40] In general, the N2200 polymer domains[40] in polymer:polymer blends are highly pure, likely due to the high crystallinity and the strong aggregation of N2200, while the donor polymer domains (e.g. PTQ1, P3HT[40]) are rather impure. Understanding full details of domain purity in polymer:polymer blends is highly challenging and requires extensive studies[37,40–42] involving Scanning Transmission X-ray Microscopy (STXM), R-SoXS, and other photophysics methods, and is outside the scope of this paper. We have compared the relative purity level of NT:N2200 blend with previously reported NT:fullerene blends (the polymer domain of NT:fullerene blends was shown to be rather impure,[37] containing at least 20–30% of fullerene impurity) based on their R-SoXS data following reported protocols.[37] The comparison indicates that the NT:N2200 blend exhibits a relative purity level that is 12% higher than that of NT:PC_{71}BM and comparable to that of NT:PC_{61}BM. The impure NT domain is consistent with the high PLQE for NT in the NT:N2200 blend and can facilitate exciton dissociation within the NT polymer domains. Similar to the NT:PC_{71}BM system,[37] the impure nature of NT domains is likely the reason why NT:N2200 can yield high PSC efficiencies despite of the relatively large domain size. Lastly, the NT:N2200 film coated from a less polar solvent, tetralin, showed a multi-length scale structure (R-SoXS

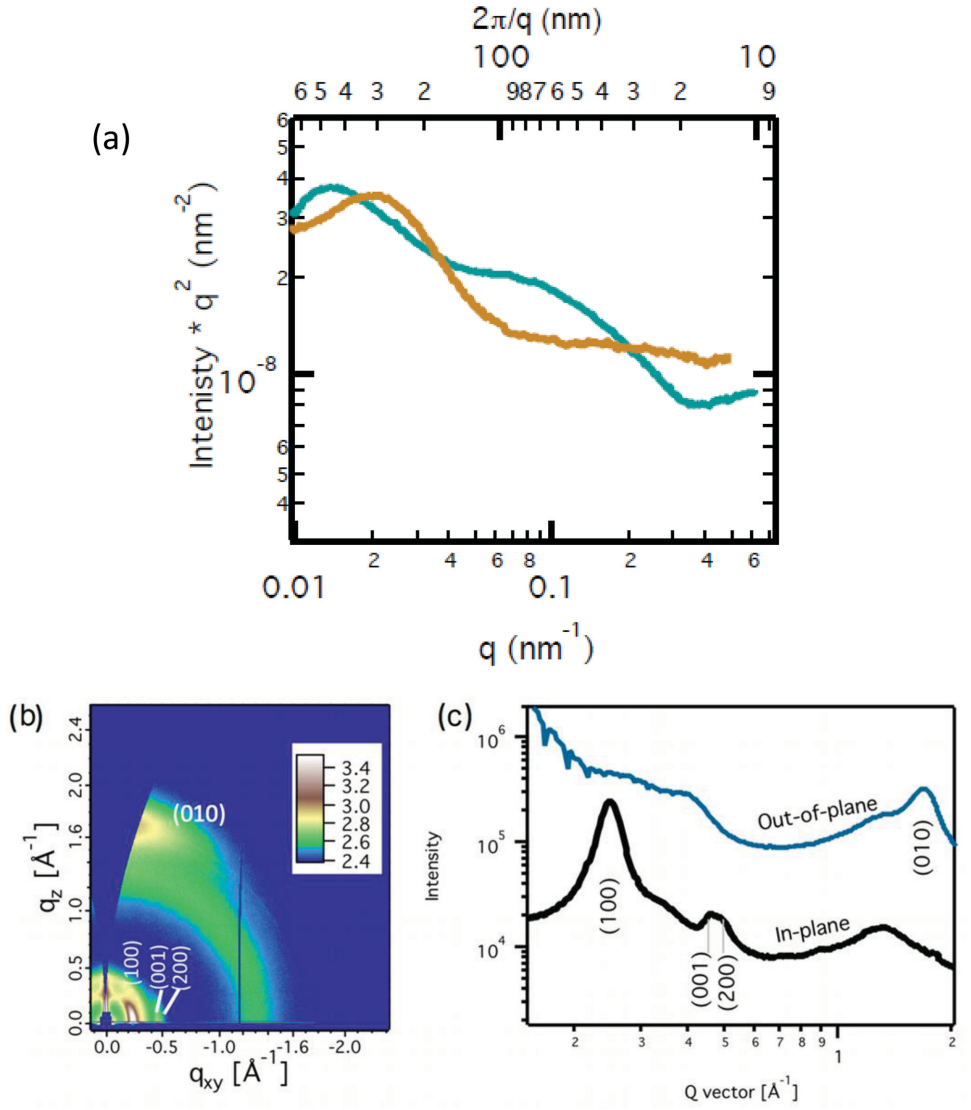

Figure 3. (a) R-SoXS profile of NT:N2200 blend films processed from DCB (brown line) and tetralin (green line). (b) GIWAXS 2D pattern of a NT:N2200 blend film; (c) 1-D scattering profile of the same NT:N2200 blend film.

profile shown in Figure 3a, blue line) with domain spacing at 500 and 90 nm. It appears that such multi-length scale structure with domains larger then the film thickness is not hierarchical and has some negative impact on performance, likely due to the formation of domains in which the optimum D/A ratio is no longer preserved. This outcome is reasonable considering that tetralin is a relatively poor solvent (compared to DCB), in which NT and N2200 exhibit stronger aggregation and thus form larger polymer domains.

Grazing incident wide-angle X-ray scattering (GIWAXS) was employed to examine the polymer molecular packing/aggregation. First, the GIWAXS pattern of a neat NT film is shown in Figure S3a and the GIWAXS patterns of pure N2200,[43,44] PTB7:N2200[43] and NT:$PC_{71}BM$[37] films have been reported previously. The N2200 neat film typically exhibits (100), (001), and possibly (200) peaks at ~0.25–0.26, 0.45, and 0.50–0.52 $Å^{-1}$, respectively along q_{xy} and a (010) peak at ~1.6 $Å^{-1}$ along q_z. The (010) peak at q_z of 1.6 $Å^{-1}$ was also observed for N2200 in PTB7:N2200 blend films.[43] The NT polymer, in either neat films or NT:PCBM blend films[37], exhibits (100) and possibly (200) peaks at ~0.25 and 0.50 $Å^{-1}$ along q_{xy} and a clear (010) peak at ~1.75 $Å^{-1}$ along q_z. Figure 3b, 3c show 2D scattering patterns and scattering profiles of the in-plane (black line) and out-of plane directions (blue line) of a NT:N2200 film, which exhibits, along q_{xy}, a sharp scattering peak at ~0.25 $Å^{-1}$ and a double peak at ~0.45–0.5 $Å^{-1}$. While the peak at 0.45 $Å^{-1}$ can be assigned to the (001) diffraction of N2200, the peaks at 0.25 $Å^{-1}$ and 0.5 $Å^{-1}$ are (100) and (200) peaks that have contributions possibly from both NT and N2200. The GIWAXS profile shows a slightly broadened peak at 1.7 $Å^{-1}$ along q_z, which can be fitted into two peaks (at 1.6 and 1.75 $Å^{-1}$, Figure S4) that can be assigned to N2200 and NT, respectively. These data ((001) peak at 0.45 $Å^{-1}$ and (010) component peak at 1.6 $Å^{-1}$, Figure S4) support that N2200 is crystalline in the NT:N2200 blend. N2200 is generally found to be a highly crystalline polymer whose crystallinity and face-on orientation relative to the substrate

Adv. Mater. 2014,
DOI: 10.1002/adma.201402473

can be conserved in polymer blends[43]. The (010) component peak at 1.75 $Å^{-1}$ along q_z (also supported by hole mobility data discussed in the next paragraph) indicates that NT is also crystalline and exhibit a preferential face-on orientation that is favorable for charge transport in the vertical direction. These data indicates that there is likely no co-crystallization behavior between NT and N2200.

To further understand the charge transport ability of the NT:N2200 blend, we measured the space-charge-limited-current (SCLC) mobilities of the hole-only and electron-only devices based on NT:N2200 blend films and found that the hole mobility and electron mobility of the blend film are 2.5×10^{-4} and 6.9×10^{-4} cm^2 V^{-1} s^{-1}, respectively. The hole mobility value obtained for NT:N2200 blend is comparable to that (2.7×10^{-4} cm^2 V^{-1} s^{-1}) of NT:fullerene blend and slightly lower than that (3.9×10^{-4} cm^2 V^{-1} s^{-1}) of the pure NT film (Figure S5, Table S3). For the NT:fullerene blend film,[37] NT was found to be cystalline, and more importantly, exhibit a preferentially face-on orientation, which provides good hole transport in the NT:fullerene blend. The similarity of the hole mobility and GIWAXS data between NT:N2200 and NT:fullerene blends support that the crystallinity and hole transport ability of NT in the NT:N2200 blend are comparable to those in the NT:fullerene case. Note that the thermally annealed NT:N2200 film exhibits a significantly higher hole mobility than the un-annealed film (4×10^{-5} cm^2 V^{-1} s^{-1}), which helps to explain the lower PCE of the unannealed all-PSC device. The use of a pair of semi-crystalline polymers that can maintain their crystallinity and high charge transport ability in the bulk-heterojunction blend film is an important feature of our work that is different from previous high-efficiency all-PSCs.[9],[11] The relatively high and balanced hole and electron mobilities in the NT:N2200 system contributed to the relatively good fill factors and efficiencies of NT:N2200-based cells.

N2200 has been previously explored as the acceptor for all-PSCs as it exhibits a high electron mobility, which is considered an important factor influencing the performance of PSCs. However, studies combining N2200 with many donor polymers (e.g., P3HT, PTB7) have led to disappointing PSC efficiencies. For P3HT:N2200-based PSCs, although it exhibits efficient and balanced charge transports (hole and electron mobility both about 1×10^{-3} cm^2 V^{-1} s^{-1}), P3HT and N2200 tend to form large-scale phase segregation (as large as 1 μm), because they do not intermix well and tend to self-aggregate into large crystalline domains.[31,32] Special processing protocols[32] have been developed to suppress the aggregation of P3HT and N2200 during the film-casting process and still yielded only very low EQE values (~20%) and PCE of 1.4%. PTB7:N2200 blends[27,43] form a poor morphology containing amorphous PTB7 domains, leading to an extremely poor hole mobility of 10^{-6} cm^2 V^{-1} s^{-1} and a PCE of 2.7%. Apparently, PTB7 cannot maintain its crystallinity and charge transport ability when mixed with N2200. To reduce the polymer domain size and to increase the intermixing of donor and acceptor polymers, Ito and coworkers adopted an amorphous polymer PTQ1, which yields a PCE of 4.1% when combined with N2200.[9] However, the hole mobility of PTQ1 is very low and unbalanced with N2200, thus limiting the performance of the cell. The NT:N2200-based PSCs reported here appear to find a reasonable balance between the previously reported N2200-based all-PSCs. Compared to PTB7 and PTQ1, NT exhibits greater crystallinity, and more importantly, can maintain its crystallinity with a preferentially face-on orientation in the NT:N2200 blend film. This led to a greater hole transport ability of NT than PTB7 and PTQ1 and more balanced hole and electron transports in NT:N2200 blends. Compared to P3HT, although NT is not highly crystalline as P3HT is, NT exhibits better intermixing with N2200 than P3HT and forms a more favorable polymer:polymer blend morphology with a reasonably small domain size. The NT:N2200 all-PSCs provide an interesting direction to improve the performance of all-PSCs. Further improvements are still possible by reducing the domain size of the polymer blend and by increasing the hole mobility of the donor polymers. These can be achieved by modifying the structures of the donor and acceptor polymers to further suppress the aggregation of the acceptor polymer and slightly increase the crystallinity of the donor polymer, hence obtain a polymer blend with more favorable morphology and more balanced charge transports.

To conclude, we have demonstrated high-performance all-PSCs based on a pair of crystalline low-bandgap polymers. A high J_{sc} of 11.5 mA cm^{-2} and a PCE of up to 5% have been achieved due to the low optical bandgap of the donor polymer and the reasonably high EQE of the cell that is the result of the relatively favorable morphology of the NT:N2200 blends. R-SoXS, AFM, and TEM characterizations support that the NT:N2200 blend film is smooth and exhibits an average domain size of about 100 nm. GIWAXS and charge transport data combined indicate that NT can maintain its crystallinity with a preferential face-on orientation in the NT:N2200 blends, which lead to a hole mobility that is reasonably balanced with the electron mobility of N2200. Our morphological characterizations can largely explain the performance of NT:N2200-based all-PSCs. Our results provide important inspirations to develop high-efficiency all-PSCs based on donor polymers with low optical bandgaps.

Experimental Section

Materials: The syntheses and characterization of NT and N2200 were reported elsewhere.[35,36]

Absorption Spectra of Thin Films: The absorption spectra of NT, N2200 and NT:N2200 solid thin films were measured by a Cary 50 UV-vis spectrophotometer.

Fabrication and Characterization of Polymer Solar Cell Devices: The ITO-coated glass substrates were washed by sequential ultrasonication in water/detergent, water, acetone, and isopropanol for 30 min in each solvent. The washed substrates were further treated with a UV-O_3 cleaner (Novascan, PSD Series digital UV ozone system) for 30 min. A topcoat layer of ZnO (The diethylzinc solution 15 wt% in toluene, diluted by tetrahydrofuran) was spin-coated onto the ITO substrate at a spinning rate of 5000 rpm for 30 s and then baked in air at 150 °C for 20 min. A blend of NT:N2200 at a concentration of 8 mg mL^{-1} in DCB was prepared by stirring at 100 °C overnight. A warm (100 °C) solution of polymer blend was then spin-coated on the top of ZnO layer at different speed from 1200–1800 rpm to achieve an optimal film thickness. All dried thin film was thermally annealed at 160–180 °C for 10 min inside a N_2-filled glove box. The thickness of active layer is typically 90 nm. After that, a vanadium oxide interlayer (V_2O_5, 20 nm) and an aluminum electrode (Al, 100 nm) were vacuum-deposited at 2.0×10^{-6} torr. The current density–voltage (*J–V*) characteristics were measured in air under simulated AM

1.5G solar irradiation (100 mW cm^{-2}, Newport: Oriel model 94021A). The light intensity was adjusted by using a standard silicon reference cell with a KG5 filter. The *J–V* characteristics of the photovoltaic cells were recorded with a *J–V* measurement system (Keithley 236). The EQE measurement was performed on a Newport EQE system equipped with a standard Si diode (Oriel lamp model 74125). The configuration of the shadow mask afforded four independent devices on each substrate, and each device had an active layer of ~5.9 mm^2.

AFM Characterization: AFM measurements were performed by using a Scanning Probe Microscope-Dimension 3100 in tapping mode. All films were coated on ITO glass substrates.

Photoluminescence Quenching Measurements: PL spectra of NT:N2200 films were measured upon excitation at 670 nm. The resulting PL emission peak (at 820 nm) of NT:N2200 blend was linearly fitted into two component peaks (at 780 and 840 nm) that precisely match the PL spectra of NT and N2200 control samples. The PLQE of NT was calculated based on the PL intensity of the NT component of the NT:N2200 PL spectrum and the PL intensity of NT control sample. The PLQE of N2200 was calculated similarly.

Grazing Incidence Wide-Angle X-ray Scattering (GIWAXS) Characterization: GIWAXS measurements were performed at beamline 7.3.3 at the Advanced Light Source.[45] Samples were prepared using identical blend solutions as those used in devices on Si substrate. The 10 keV X-ray beam was incident at a grazing angle of 0.12°–0.16°, which maximized the scattering intensity from the samples. The scattered X-rays were detected using a Dectris Pilatus 1M photon counting detector.

Resonant Soft X-ray Scattering (R-SoXS): R-SoXS transmission measurements were performed at beamline 11.0.1.2 at the Advanced Light Source (ALS).[46] Samples for R-SoXS measurements were prepared on a PSS modified Si substrate under the same conditions as those used for device fabrication, and then transferred by floating in water to a 1.5 mm × 1.5 mm, 100 nm thick Si_3N_4 membrane supported by a 5 mm × 5 mm, 200 μm thick Si frame (Norcada Inc.). 2-D scattering patterns were collected on an in-vacuum CCD camera (Princeton Instrument PI-MTE). The sample detector distance was calibrated from diffraction peaks of a triblock copolymer poly(isoprene-b-styrene-b-2-vinyl pyridine), which has a known spacing of 391 Å. The beam size at the sample is approximately 100 μm by 200 μm.

Supporting Information

Supporting Information is available from the Wiley Online Library or from the author.

Acknowledgements

We thank the Ministry of Science and Technology through project No.2013CB834701 and No.2014CB643501, Hong Kong ITC for financial support through project ITS/354/12 and Hong Kong RGC through project N_HKUST623/13. Fei Huang, Peng Liu and Kai Zhang acknowledge funding by the Natural Science Foundation of China (No. 21125419 and 51361165301). X-ray characterization by NCSU supported by the U.S. Department of Energy, Office of Science, Basic Energy Science, Division of Materials Science and Engineering under Contract DE-FG02-98ER45737. X-ray data was acquired at beamlines 11.0.1.2, 7.3.3 and 5.3.2.2 at the Advanced Light Source, which is supported by the Director, Office of Science, Office of Basic Energy Sciences, of the U.S. Department of Energy under Contract No. DE-AC02-05CH11231.

Received: June 3, 2014
Revised: August 5, 2014
Published online:

[1] G. Yu, J. Gao, J. C. Hummelen, F. Wudl, A. J. Heeger, *Science* **1995**, *270*, 1789.
[2] J. J. M. Halls, C. A. Walsh, N. C. Greenham, E. A. Marseglia, R. H. Friend, S. C. Moratti, A. B. Holmes, *Nature* **1995**, *376*, 498.
[3] Z. C. He, C. M. Zhong, S. J. Su, M. Xu, H. B. Wu, Y. Cao, *Nat. Photon.* **2012**, *6*, 591.
[4] J. B. You, L. T. Dou, K. Yoshimura, T. Kato, K. Ohya, T. Moriarty, K. Emery, C. C. Chen, J. Gao, G. Li, Y. Yang, *Nat. Commun.* **2013**, *4*, 1446.
[5] Y. Vaynzof, T. J. K. Brenner, D. Kabra, H. Sirringhaus, R. H. Friend, *Adv. Funct. Mater.* **2012**, *22*, 2418.
[6] D. Mori, H. Benten, H. Ohkita, S. Ito, K. Miyake, *ACS Appl. Mater. Interfaces* **2012**, *4*, 3325.
[7] T. Earmme, Y. J. Hwang, N. M. Murari, S. Subramaniyan, S. A. Jenekhe, *J. Am. Chem. Soc.* **2013**, *135*, 14960.
[8] E. Zhou, J. Cong, K. Hashimoto, K. Tajima, *Adv. Mater.* **2013**, *25*, 6991.
[9] D. Mori, H. Benten, I. Okada, H. Ohkita, S. Ito, *Adv. Energy Mater.* **2014**, *4*, 1301006.
[10] X. W. Zhan, Z. A. Tan, B. Domercq, Z. S. An, X. Zhang, S. Barlow, Y. F. Li, D. B. Zhu, B. Kippelen, S. R. Marder, *J. Am. Chem. Soc.* **2007**, *129*, 7246.
[11] Y. Zhou, T. Kurosawa, W. Ma, Y. Guo, L. Fang, K. Vandewal, Y. Diao, C. Wang, Q. Yan, J. Reinspach, J. Mei, A. L. Appleton, G. I. Koleilat, Y. Gao, S. C. B. Mannsfeld, A. Salleo, H. Ade, D. Zhao, Z. Bao, *Adv. Mater.* **2014**, *26*, 3767.
[12] T. W. Holcombe, J. E. Norton, J. Rivnay, C. H. Woo, L. Goris, C. Piliego, G. Griffini, A. Sellinger, J. L. Bredas, A. Salleo, J. M. J. Frechet, *J. Am. Chem. Soc.* **2011**, *133*, 12106.
[13] J. T. Bloking, X. Han, A. T. Higgs, J. P. Kastrop, L. Pandey, J. E. Norton, C. Risko, C. E. Chen, J. L. Bredas, M. D. Mcgehee, A. Sellinger, *Chem. Mater.* **2011**, *23*, 5484.
[14] C. H. Woo, T. W. Holcombe, D. A. Unruh, A. Sellinger, J. M. J. Frechet, *Chem. Mater.* **2010**, *22*, 1673.
[15] R. Y. C. Shin, T. Kietzke, S. Sudhakar, A. Dodabalapur, Z. K. Chen, A. Sellinger, *Chem. Mater.* **2007**, *19*, 1892.
[16] T. Kietzke, R. Y. C. Shin, D. A. M. Egbe, Z. K. Chen, A. Sellinger, *Macromolecules* **2007**, *40*, 4424.
[17] R. Y. C. Shin, P. Sonar, P. S. Siew, Z. K. Chen, A. Sellinger, *J. Org. Chem.* **2009**, *74*, 3293.
[18] K. H. Hendriks, G. H. L. Heintges, V. S. Gevaerts, M. M. Wienk, R. A. J. Janssen, *Angew. Chem. Int. Ed.* **2013**, *52*, 8341.
[19] T. B. Yang, M. Wang, C. H. Duan, X. W. Hu, L. Huang, J. B. Peng, F. Huang, X. Gong, *Energy Environ. Sci.* **2012**, *5*, 8208.
[20] Y. Y. Liang, L. P. Yu, *Acc. Chem. Res.* **2010**, *43*, 1227.
[21] C. Piliego, T. W. Holcombe, J. D. Douglas, C. H. Woo, P. M. Beaujuge, J. M. J. Frechet, *J. Am. Chem. Soc.* **2010**, *132*, 7595.
[22] C. Cabanetos, A. El Labban, J. A. Bartelt, J. D. Douglas, W. R. Mateker, J. M. J. Frechet, M. D. Mcgehee, P. M. Beaujuge, *J. Am. Chem. Soc.* **2013**, *135*, 4656.
[23] S. C. Price, A. C. Stuart, L. Q. Yang, H. X. Zhou, W. You, *J. Am. Chem. Soc.* **2011**, *133*, 4625.
[24] H. Y. Chen, J. H. Hou, S. Q. Zhang, Y. Y. Liang, G. W. Yang, Y. Yang, L. P. Yu, Y. Wu, G. Li, *Nat. Photon.* **2009**, *3*, 649.
[25] X. G. Guo, N. J. Zhou, S. J. Lou, J. Smith, D. B. Tice, J. W. Hennek, R. P. Ortiz, J. T. L. Navarrete, S. Y. Li, J. Strzalka, L. X. Chen, R. P. H. Chang, A. Facchetti, T. J. Marks, *Nat. Photon.* **2013**, *7*, 825.
[26] S. Fabiano, S. Himmelberger, M. Drees, Z. Chen, R. M. Altamimi, A. Salleo, M. A. Loi, A. Facchetti, *Adv. Energy Mater.* **2013**, *4*, 1301409.
[27] N. Zhou, H. Lin, S. J. Lou, X. Yu, P. Guo, E. F. Manley, S. Loser, P. Hartnett, H. Huang, M. R. Wasielewski, L. X. Chen, R. P. H. Chang, A. Facchetti, T. J. Marks, *Adv. Energy Mater.* **2013**, *4*, 1300785.

DOI: 10.1002/adma.201402473

[28] S. Fabiano, Z. Chen, S. Vahedi, A. Facchetti, B. Pignataro, M. A. Loi, *J. Mater. Chem.* **2011**, *21*, 5891.
[29] H. P. Yan, B. A. Collins, E. Gann, C. Wang, H. Ade, C. R. Mcneill, *ACS Nano* **2012**, *6*, 677.
[30] B. Friedel, C. R. Mcneill, N. C. Greenham, *Chem. Mater.* **2010**, *22*, 3389.
[31] J. R. Moore, S. Albert-Seifried, A. Rao, S. Massip, B. Watts, D. J. Morgan, R. H. Friend, C. R. Mcneill, H. Sirringhaus, *Adv. Energy Mater.* **2011**, *1*, 230.
[32] M. Schubert, D. Dolfen, J. Frisch, S. Roland, R. Steyrleuthner, B. Stiller, Z. H. Chen, U. Scherf, N. Koch, A. Facchetti, D. Neher, *Adv. Energy Mater.* **2012**, *2*, 369.
[33] K. Schmidt, C. J. Tassone, J. R. Niskala, A. T. Yiu, O. P. Lee, T. M. Weiss, C. Wang, J. M. J. Fréchet, P. M. Beaujuge, M. F. Toney, *Adv. Mater.* **2014**, *26*, 300.
[34] J. A. Bartelt, J. D. Douglas, W. R. Mateker, A. E. Labban, C. J. Tassone, M. F. Toney, J. M. J. Fréchet, P. M. Beaujuge, M. D. Mcgehee, *Adv. Energy Mater.* **2014**, *4*, 1301733.
[35] M. Wang, X. W. Hu, P. Liu, W. Li, X. Gong, F. Huang, Y. Cao, *J. Am. Chem. Soc.* **2011**, *133*, 9638.
[36] H. Yan, Z. H. Chen, Y. Zheng, C. Newman, J. R. Quinn, F. Dotz, M. Kastler, A. Facchetti, *Nature* **2009**, *457*, 679.
[37] W. Ma, J. R. Tumbleston, M. Wang, E. Gann, F. Huang, H. Ade, *Adv. Energy Mater.* **2013**, *3*, 864.
[38] D. Chen, F. Liu, C. Wang, A. Nakahara, T. P. Russell, *Nano Lett.* **2011**, *11*, 2071.
[39] W. Ma, L. Ye, S. Q. Zhang, J. H. Hou, H. Ade, *J. Mater. Chem. C* **2013**, *1*, 5023.
[40] M. Schubert, B. A. Collins, H. Mangold, I. A. Howard, W. Schindler, K. Vandewal, S. Roland, J. Behrends, F. Kraffert, R. Steyrleuthner, Z. Chen, K. Fostiropoulos, R. Bittl, A. Salleo, A. Facchetti, F. Laquai, H. W. Ade, D. Neher, *Adv. Funct. Mater.* **2014**, *24*, 4068.
[41] S. Albrecht, S. Janietz, W. Schindler, J. Frisch, J. Kurpiers, J. Kniepert, S. Inal, P. Pingel, K. Fostiropoulos, N. Koch, D. Neher, *J. Am. Chem. Soc.* **2012**, *134*, 14932.
[42] J. R. Tumbleston, A. C. Stuart, E. Gann, W. You, H. Ade, *Adv. Funct. Mater.* **2013**, *23*, 3463.
[43] Y. Q. Tang, C. R. Mcneill, *J. Polym. Sci. Part B: Polym. Phys.* **2013**, *51*, 403.
[44] J. Rivnay, M. F. Toney, Y. Zheng, I. V. Kauvar, Z. H. Chen, V. Wagner, A. Facchetti, A. Salleo, *Adv. Mater.* **2010**, *22*, 4359.
[45] A. Hexemer, W. Bras, J. Glossinger, E. Schaible, E. Gann, R. Kirian, A. Macdowell, M. Church, B. Rude, H. Padmore, *J. Phys. Conf. Ser.* **2010**, *247*, 012007.
[46] E. Gann, A. T. Young, B. A. Collins, H. Yan, J. Nasiatka, H. A. Padmore, H. Ade, A. Hexemer, C. Wang, *Rev. Sci. Instrum.* **2012**, *83*, 045110.